

AN EXPERIMENTAL AND THEORETICAL STUDY OF STRUCTURAL DAMPING

IN COMPLIANT FOIL BEARINGS

C.-P. Roger Ku
Mechanical Technology Incorporated
Latham, New York

578-37

12862

P-11

ABSTRACT

This paper describes an experimental investigation into the dynamic characteristics of corrugated foil (bump foil) strips used in compliant surface foil bearings. This study provided the first opportunity to quantify the structural damping of bump foil strips. The experimental data were compared to results obtained by a theoretical model developed earlier. The effects of bearing design parameters, such as static loads, dynamic displacement amplitudes, bump configurations, pivot locations, surface coatings, and lubricant were also evaluated. An understanding of the dynamic characteristics of bump foil strips resulting from this work offers designers a means for enhancing the design of high-performance compliant foil bearings.

INTRODUCTION

Over the past 10 years, the ability of a conventional bearing to survive the rigors of today's advanced turbine engines and rocket propulsion systems has gradually declined. Extreme environments are pushing conventional liquid fluid-film bearings to, or perhaps beyond, their operating limits within high-temperature and cryogenic settings. In some turbine engines, bearing temperatures are expected to exceed the capabilities of conventional liquid lubricants completely; in rocket propulsion, bearing deficiencies persist in cryogenic turbopumps. On the other hand, compliant foil bearings, which can operate on either gas or liquid, have demonstrated good performance at elevated temperatures and high speeds, and are very attractive for use with cryogenic fluids.

The resilience offered by a compliant foil bearing stems from its construction of a smooth top foil, which provides the bearing surface, and a flexible, corrugated bump foil strip, which provides a resilient support to the top foil (see Figure 1). The bump foil strip is welded at one end to the bearing housing and is free at the other end. The advantages offered by the compliant foil bearing over conventional bearings include its adaptation to shaft misalignment, variations due to tolerance build-ups, centrifugal shaft growth, and differential thermal expansion. It has long life and reliability, higher load capacity, a lower power loss, and superior rotordynamic characteristics [1].

Existing analytical models of foil bearings are not as developed, however, as those of conventional-type fluid-film bearings. Walowit et al. [2] first introduced a theoretical model to determine the static structural stiffness of the resilient support. This model assumed that bumps do not interact with each other, thus neglecting local interactive forces between bumps as well as friction forces between the top foil and the bumps. According to this model, when the top foil is loaded, each bump has identical deflection and static stiffness.

Ku and Heshmat [3] recently developed a theoretical model to investigate the mechanism of deformation of a bump foil strip used in thrust foil bearings. This work was a first step toward

understanding the relationship between frictional and local interacting forces in bump foil strips. In this model, the friction forces between top foil and bumps, the friction forces between housing and bumps, and the local interactive forces between bumps are taken into consideration. These researchers predicted that the bumps near the fixed end would have higher static stiffness than the bumps near the free end, and that the load distribution profile would have a great effect on bump local static stiffness. More recently, Ku and Heshmat [4,5] extended their model to predict the dynamic structural stiffness and equivalent viscous damping coefficients of the resilient support, the bump foil strip, in a journal bearing or damper. The stiffness is calculated based on the perturbation of the journal center with respect to its static equilibrium position. The equivalent viscous damping coefficient is determined based on the area of a closed hysteresis loop of the journal center motion. With the introduction of this enhanced model, the analytical tools are now available for the design of compliant foil bearings.

In a follow-up experimental investigation [6,7], the two-dimensional deflections of bump foil strips were studied via an optical tracking system to verify the feasibility of the theoretical model. The static and dynamic structural stiffness of bump foil strips were measured and compared to theoretical predictions. The comparisons show very good agreement. The friction coefficients between the contact surfaces for different surface coatings were also determined empirically by matching the values of dynamic structural stiffness. It was reported that the dynamic structural stiffness is static load and/or dynamic amplitude dependent.

In this paper, the experimental study has been extended to quantify the equivalent viscous damping coefficients of bump foil strips. The results are compared to analytical predictions. The effects of static load, dynamic displacement amplitude, bump configurations, pivot locations and surface coatings are also investigated.

EXPERIMENTAL SETUP

The test apparatus and bump foil assembly are shown in Figures 2 and 3. Each pad is 41.1 mm by 24.6 mm and made of steel. The lower pad acts as a housing and the upper pad is supported by a bump foil strip. The bump foil strip is welded at one end of the lower pad; a smooth top foil is welded on the lower surface of the upper pad. As the lower pad moves or vibrates in the vertical direction, the bumps are deformed in both vertical and horizontal directions. The vertical deflections of the bumps determine load capacity, or stiffness, and the horizontal motions of the bumps yield damping.

A horizontal hard dowel, which acts as a pivot, is placed between a circular plate and the upper pad. The pivot can be located in any one of five grooves that are spaced 3.96 mm apart on the top surface of the upper pad. A vertical dowel, inserted tightly into the circular plate and loosely into the upper pad, prevents the horizontal motion of the upper pad. When the pivot location is changed, the upper and lower pads move as a unit.

The lower pad is mounted on the lower adaptor by two roll pins. The circular plate with a central groove is fixed on the upper adaptor. The upper and lower adaptors are mounted on an MTS hydraulic force control system. An extensometer, which has a sensitivity of 25 $\mu\text{m}/\text{V}$, controls the relative distance between the adaptors. A force transducer (44.5 N/V) measures the load capacity of the bump foil strip. The optical tracking system used for the static deformation study [6] was removed. An Ono-Sokki two-channel analyzer and a plotter record the test data.

The bump foil strips and smooth top foils were made of Inconel X750; all the other parts were made of steel. Each bump foil strip is 24.1 mm wide and has six bumps. The surfaces of some of the foils were coated with either Teflon or copper. For the bump foil strip with one of these coatings, another smooth foil with the same coating was welded between the bump foil strip and the upper surface of the lower pad (see Figure 2, Surface 4). In this way, all contact surfaces had the same coating. For each coating, both dry contact surfaces and surfaces lubricated with light turbine oil were tested. Table 1 shows the configurations and coatings of the tested bump foils.

The detailed experimental procedures used to conduct the static load test were described in Reference 6. After a static load was applied, a dynamic force or displacement was imposed. In the current experiments, a dynamic displacement of the vertical deformation of the bump foil strip at the pivot location was controlled by the extensometer, and the corresponding dynamic force was recorded. Dynamic load-deflection curves (hysteresis loops) were plotted with respect to the static equilibrium positions. For each bump foil strip specimen listed in Table 1, three most centrally located pivot positions were evaluated (see Figure 2). At each pivot location, two static loads (90 and 135 N) and two dynamic displacement amplitudes (~ 2.5 and $5.0 \mu\text{m}$) at 1 Hz frequency were tested, respectively. The test parameters are shown in Table 2.

RESULTS AND DISCUSSIONS

The measured equivalent viscous damping coefficient was calculated based on the area of a hysteresis loop, A , of the pivot location and the following equation:

$$B = A / (\pi \Omega \delta^2) \quad (1)$$

The analytical result was calculated by the same equation but the hysteresis loop of the pivot location was determined by using the earlier developed theoretical model [3-5]. The experimental results are displayed in Figures 4 through 6. The resulting data points are represented by numbers, which are identical to the test number shown in the first column of Table 1. The dimensionless variables shown in the figures are defined as follows:

$$\text{Dimensionless displacement amplitude, } \delta^* = \delta \frac{E_B}{2W_T(1-\nu_B^2)} \left(\frac{t_{Br}}{\ell_r}\right)^3 \quad (2)$$

$$\text{Dimensionless structural damping, } B^* = \Omega B \frac{2(1-\nu_B^2)}{m u_B E_B} \left(\frac{\ell_r}{t_{Br}}\right)^3 \quad (3)$$

where E_B , ν_B , t_{Br} , ℓ_r , W_T , and m are known parameters (see Table 2 and Nomenclature).

Although it is very difficult to measure the friction coefficients accurately for different surface coatings, these coefficients are required as input parameters in the theoretical model. Therefore, the sum of the friction coefficients between Surfaces 1 and 2 and Surfaces 3 and 4 (Figure 2) was treated as unknown parameters, and the coefficients were determined empirically by matching the dynamic structural stiffness [7]. It was found that the Ni-Tef (or Tef-Ni) surface coating has a total friction coefficient near 0.4; the Ni-Ni surface coating has a total friction coefficient near 0.5; and the Ni-Cu (or Cu-Ni) surface coating has a total friction coefficient near 0.6. The results of structural damping for different total friction coefficients were plotted by the solid lines in Figures 4 through 6.

Figure 4 displays the effect of surface coatings and lubricant on structural damping at different static loads and dynamic displacement amplitudes. For each of the seven cases (1-7), the bump had a 4.6-mm pitch and a 76- μm thickness, and the pivot was in the center position. In general, the coating with a higher friction coefficient provides higher structural damping, however, there are exceptions when dynamic displacement amplitude is small. In comparing the experimental data with the theoretical results, the theoretical predictions always overestimate the structural damping, especially at the small dynamic displacement amplitudes. In detailed examination of both measured and calculated hysteresis loops, the measured loop does not follow the predicted one with a stick-slip condition [7]. Therefore, the area of the measured hysteresis loop is smaller than the predicted one.

Figure 5 displays the effect of three bump configurations on structural damping. For each configuration, the pivot was located in the center for a Ni-Ni surface coating with (cases 2 and 9) and without (cases 1, 8, and 10) lubricant. The theoretical results were calculated with total friction coefficients 0.6. At both static loads and dynamic displacement amplitudes, increasing the bump thickness and/or pitch would increase a small amount of structural damping. Again, the theoretical predictions overestimate the structural damping for all three bump configurations.

The effect of pivot location on structural damping is shown in Figure 6. For each pivot location, center or left, the bump had a 4.6-mm pitch, a 76- μm thickness, and a Ni-Ni surface coating with (cases C9 and L9) and without (cases C8 and L8) lubricant. The experimental data show that both pivot locations provide roughly the same amount of structural damping, which does not follow the trend of theoretical predictions. However, it is interesting to note that the theoretical results do have much better predictions for the left pivot location.

The effect of lubricant on structural damping is also shown in Figures 4 through 6. The addition of oil to the surfaces coated with nickel (cases 2 and 9) and copper (case 4) increases the damping, but not much, for most of the test conditions.

CONCLUSIONS

An experimental study was performed to quantify the structural damping of bump foil strips used in foil bearings. The results were compared to the analytical predictions by using the previously developed theoretical model. The effects of bump configurations, pivot locations, surface coatings, lubricant, static load, and dynamic displacement amplitude on the bump foil strip structural damping were also evaluated.

It was shown that the analytical predictions overestimate the structural damping for most of the test cases, especially at the small dynamic displacement amplitude. As the static load increases or dynamic displacement amplitude decreases, the structural damping does not change too much for all the test conditions. The bearing designer may use the coating with a higher friction coefficient, add the lubricant to the surfaces, and increase the bump thickness and/or pitch to achieve higher structural damping.

An understanding of the dynamic characteristics of bump foil strips resulting from this work offers designers a means for enhancing the design of high-performance compliant foil bearings. Recently, a rotor with 35 mm (1.375 in.) diameter and 15.2 N (3.4 lb) weight has been operated with two air

foil bearings to 132,000 rpm successfully. These bearings have demonstrated a load capacity to 0.67 MPa (97 psi) [8].

ACKNOWLEDGMENTS

The work was principally supported by Mechanical Technology Incorporated. The author expresses his appreciation to the organization for their support. The author would also like to thank his colleagues, Mr. M. Tomaszewski, for his help in preparing the test facilities, and Dr. H. Heshmat for his many valuable suggestions and discussions.

NOMENCLATURE

A	Hysteresis loop area of the pivot location
B	Bump foil strip structural damping
B*	Dimensionless bump foil strip structural damping
E _B	Bump elastic modulus
W	Bearing static load
ΔW	Bearing dynamic load
W _T	Unit load along transverse direction = 175 N/m (1 lb/in.)
ℓ _r	Reference bump half length = 1.27 mm (0.050 in.)
m	Number of bumps in a bump foil strip
s	Bump pitch
t _B	Bump thickness
t _{Br}	Reference bump thickness = 76.2 μm (0.003 in.)
u _B	Bump transverse length
Ω	Dynamic displacement amplitude vibration frequency
δ	Dynamic displacement amplitude of bearing pivot location
δ*	Dimensionless dynamic displacement amplitude of bearing pivot location
τ	Time
ν _B	Poisson's ratio of bump

REFERENCES

1. Gray, S., Heshmat, H., and Bhushan, B., 1981, "Technology Progress on Compliant Foil Air Bearing Systems for Commercial Applications," 8th International Gas Bearing Symposium, pp. 69-97.
2. Walowit, J. A., Murray, S. F., McCabe, J., Arwas, E. B., and Moyer, T., 1973, "Gas Lubricated Foil Bearing Technology Development for Propulsion and Power Systems," Air Force Aero Propulsion Laboratory, Wright-Patterson Air Force Base, Ohio, AFAPL-TR-73-92.
3. Ku, C.-P. R., and Heshmat, H., 1992, "Compliant Foil Bearing Structural Stiffness Analysis Part I: Theoretical Model - Including Strip and Variable Bump Foil Geometry," ASME, J. of Tribology, 114, 2, pp. 394-400.
4. Ku, C.-P. R., and Heshmat, H., 1993, "Structural Stiffness and Coulomb Damping in Compliant Foil Journal Bearings: Theoretical Considerations," accepted for publication in STLE Transactions and presentation at STLE Annual Meeting, May 17-20, Calgary, Canada.

5. Ku, C.-P. R., and Heshmat, H., 1993, "Structural Stiffness and Coulomb Damping in Compliant Foil Journal Bearings: Parametric Studies," accepted for publication in STLE Transactions and presentation at STLE Annual Meeting, May 17-20, Calgary, Canada.
6. Ku, C.-P. R., and Heshmat, H., 1993, "Compliant Foil Bearing Structural Stiffness Analysis Part II: Experimental Investigation," accepted for publishing in ASME, J. of Tribology, ASME paper 92-Trib-6.
7. Ku, C.-P. R., 1993, "Dynamic Structural Stiffness and Damping Coefficient in Compliant Foil Thrust Bearings - Comparison between Experimental and Theoretical Results," submitted to ASME J. of Tribology and ASME/STLE Joint Tribology Conference, Oct. 24-27, New Orleans, Louisiana.
8. Heshmat, H., 1993, "The Advancement in Performance of Aerodynamic Foil Journal Bearings: High Speed and Load Capability," submitted to ASME J. of Tribology and ASME/STLE Joint Tribology Conference, Oct. 24-27, New Orleans, Louisiana.

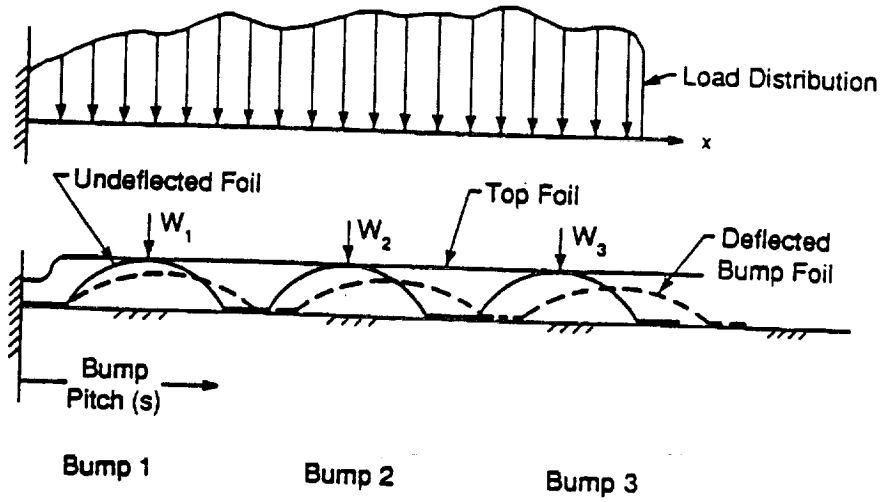
Table 1 Configurations and surface coatings of tested bumps

Test #	Pitch mm	Thickness μm	Height mm	Material Combination		Lubricant
				Surfaces 1 & 2	Surfaces 3 & 4	
1	4.572	76.2	0.4953	Ni-Ni	Ni-Steel	Air
2	4.572	76.2	0.4953	Ni-Ni	Ni-Steel	Oil
3	4.572	76.2	0.4953	Ni-Ni	Cu-Cu*	Air
4	4.572	76.2	0.4953	Ni-Ni	Cu-Cu*	Oil
5	4.572	76.2	0.4953	Cu-Cu*	Ni-Steel	Air
6	4.572	76.2	0.4953	Tef-Tef [#]	Ni-Steel	Air
7	4.572	76.2	0.4953	Ni-Ni	Tef-Tef [#]	Air
8	4.572	63.5	0.4890	Ni-Ni	Ni-Steel	Air
9	4.572	63.5	0.4890	Ni-Ni	Ni-Steel	Oil
10	4.191	76.2	0.4699	Ni-Ni	Ni-Steel	Air

- * INC-X750 Coated with Cu
- # INC-X750 Coated with PTFE

Table 2 Test parameters

Parameter	Symbol	English Unit	SI Unit
Static Load	W	20, 30 lb	90, 145 N
Perturbation Amplitude (Half)	δ	$\sim 0.0001-0.0002$ in.	$\sim 2.5-5.0$ μm
Perturbation Frequency	Ω	1 Hz	---
Number of Bumps	m	6	---
Bump Elastic Modulus	E_B	3.0×10^7 psi	2.07×10^5 MPa
Bump Poisson's Ratio	ν_B	0.25	---
Bump Transverse Length	u_B	0.95 in.	24.1 mm



901070-2

Figure 1 Bump foil strip with and without applied load

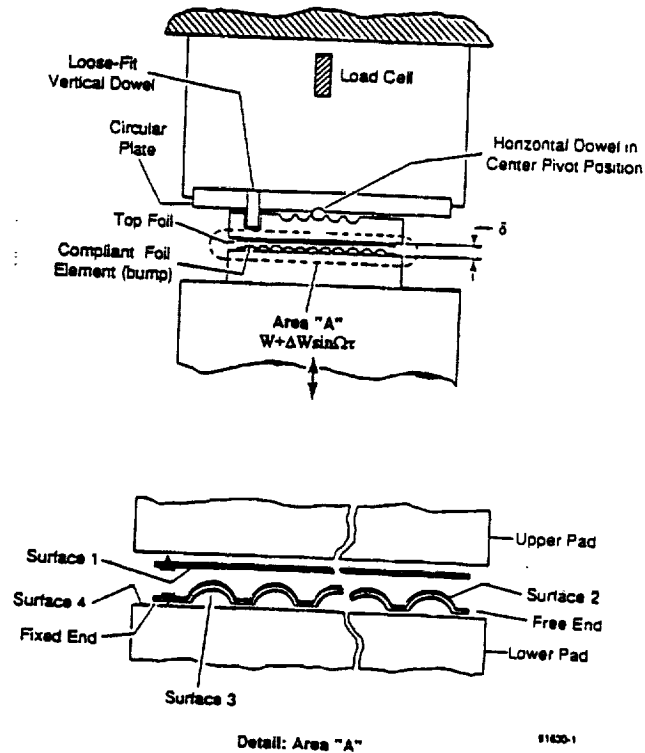


Figure 2 Bump foil pivot locations and identification of surface contacts

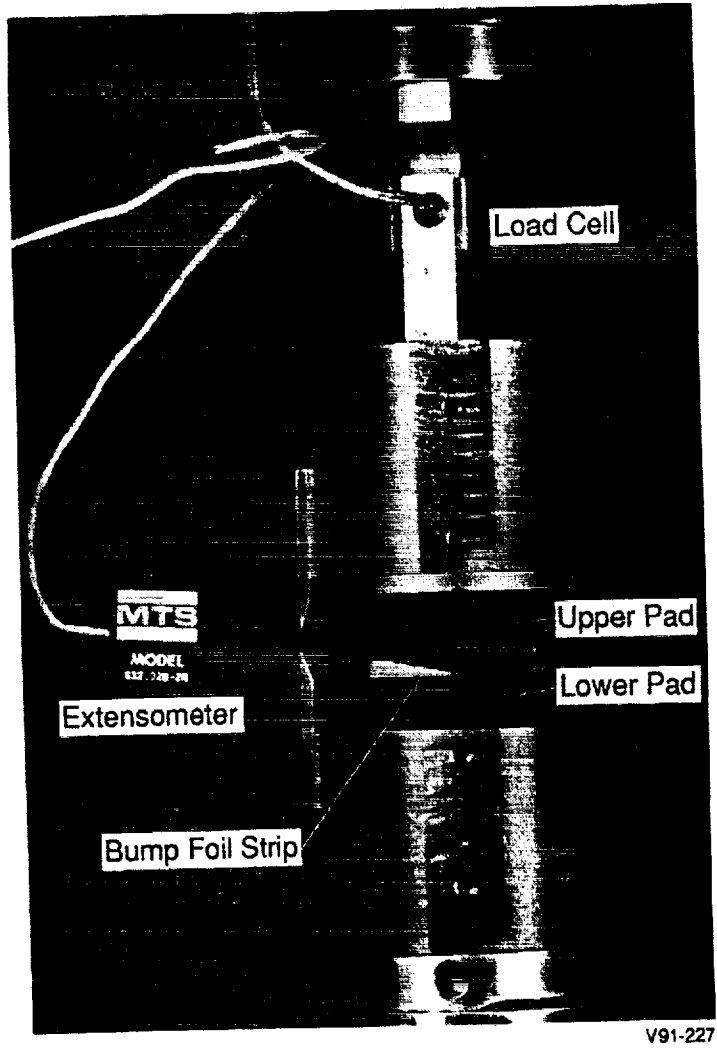
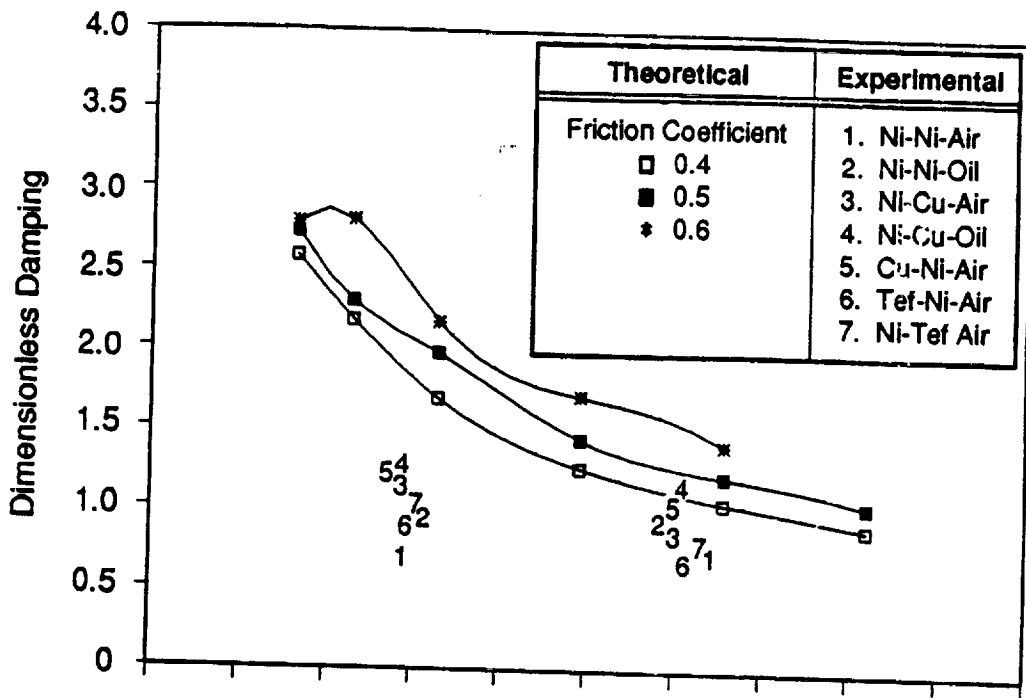
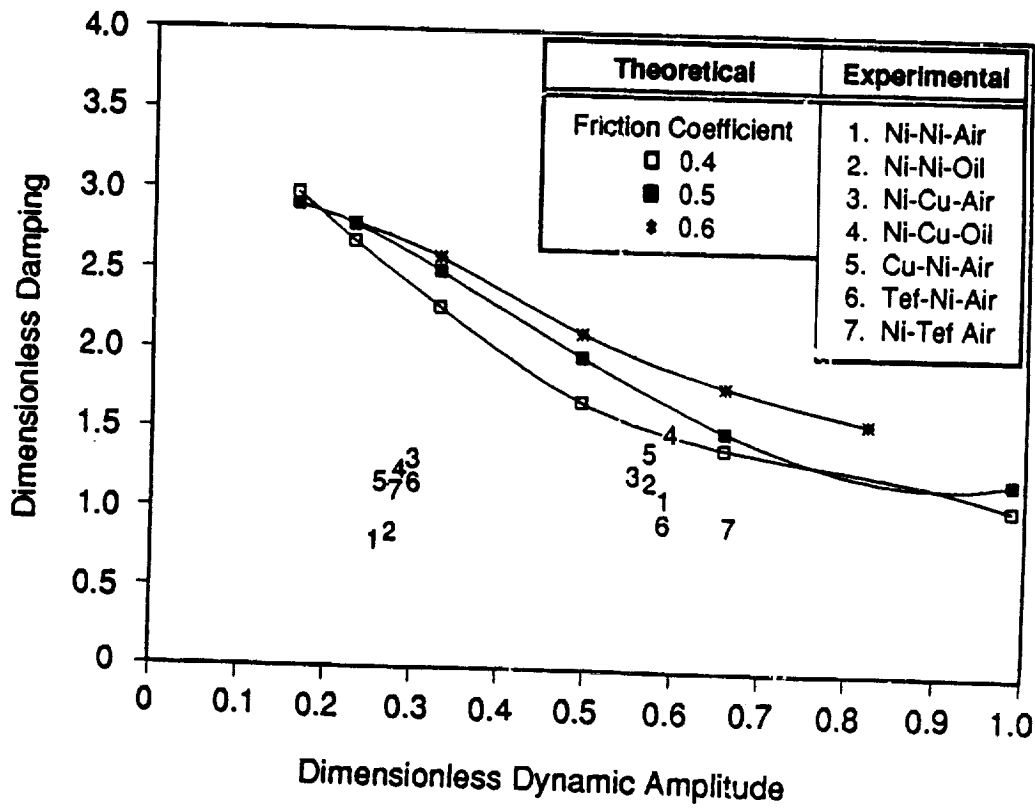


Figure 3 Close-up of bump foil assembly on test

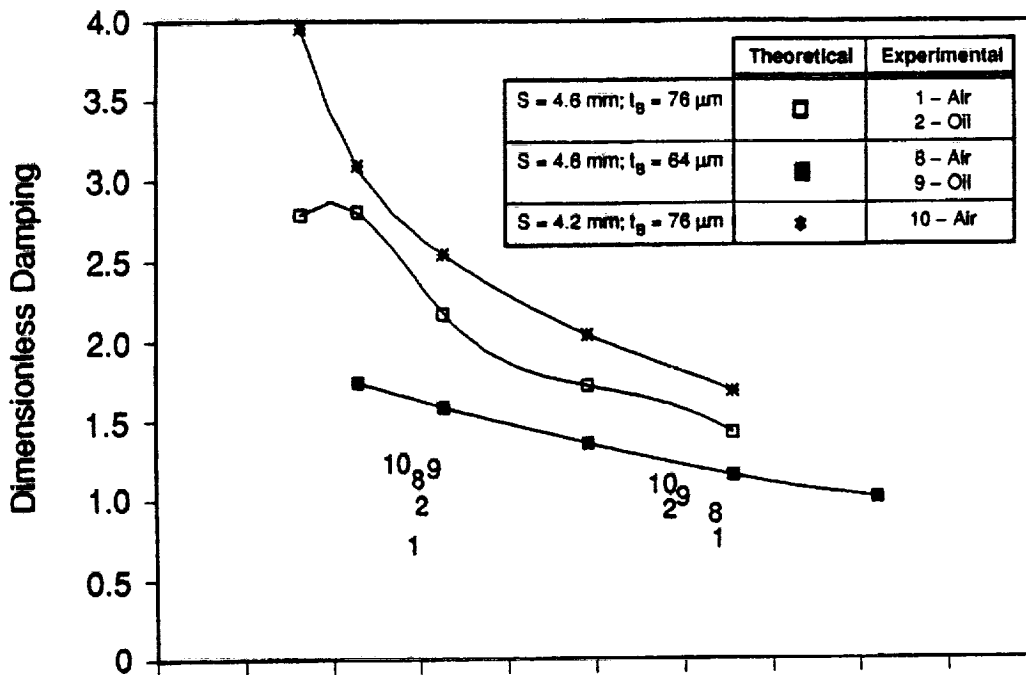


a) $W = 90 \text{ N}$

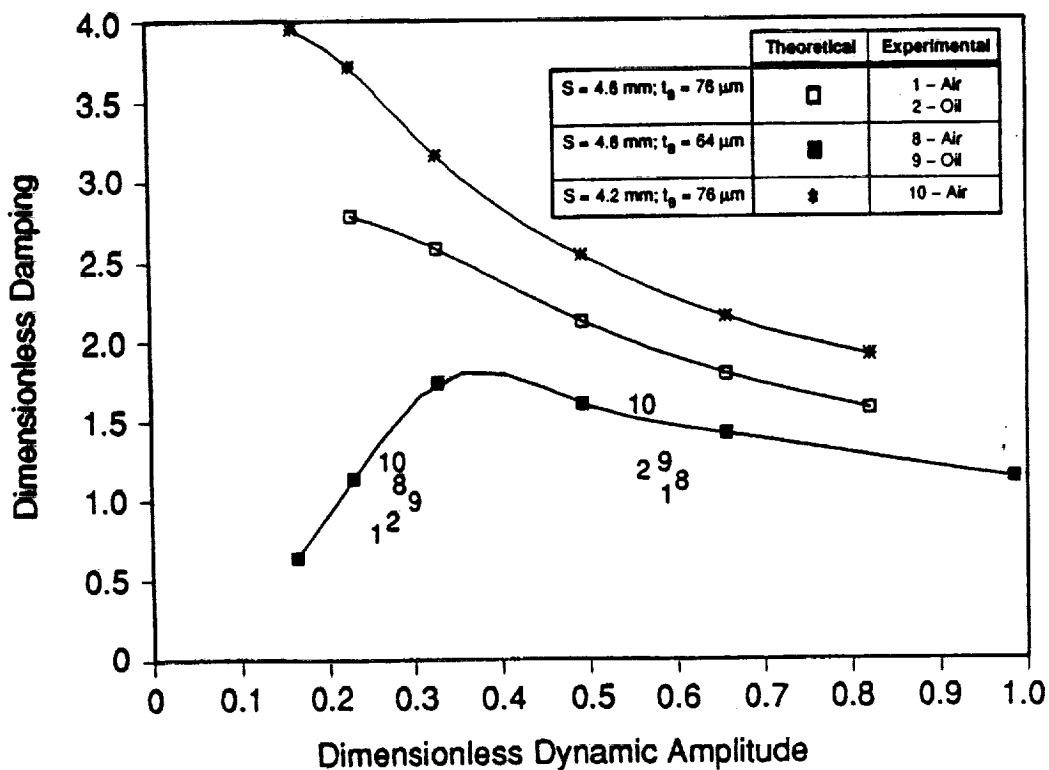


b) $W = 135 \text{ N}$

Figure 4 Effect of surface coatings on structural damping ($s=4.6 \text{ mm}$, $t_B=76 \mu\text{m}$, center pivot)

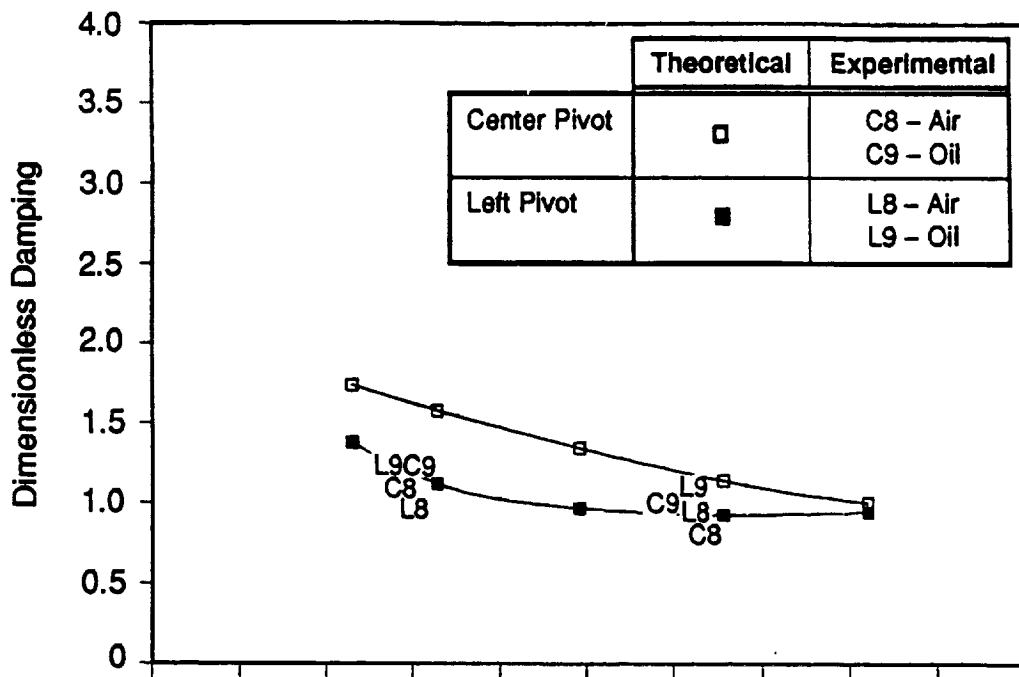


a) $W = 90 \text{ N}$

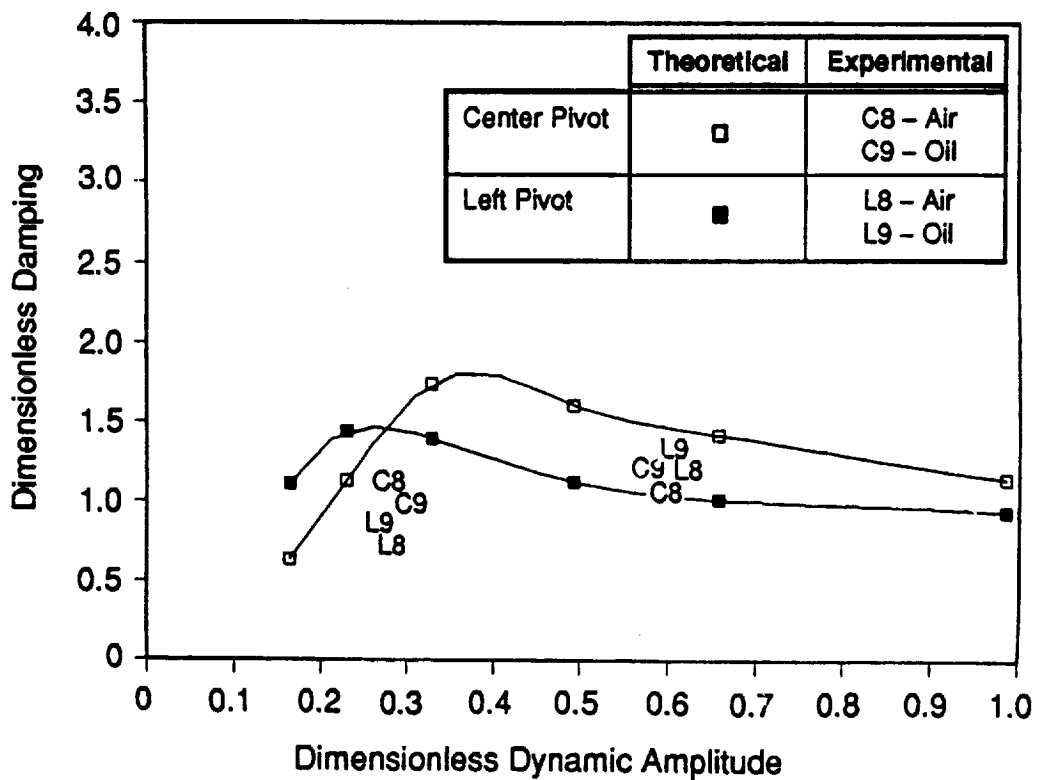


b) $W = 135 \text{ N}$

Figure 5 Effect of bump configurations on structural damping (Ni-Ni surface coating, center pivot)



a) $W = 90 \text{ N}$



b) $W = 135 \text{ N}$

Figure 6 Effect of pivot locations on structural damping
($s=4.6 \text{ mm}$, $t_B=76 \text{ }\mu\text{m}$, Ni-Ni surface coating)

